A double seismic zone in the subducting Juan Fernandez Ridge of the Nazca Plate (32°S), central Chile,

M. Marot, T. Monfret, M. Pardo, G. Ranalli, G. Nolet

▶ **To cite this version:**

M. Marot, T. Monfret, M. Pardo, G. Ranalli, G. Nolet. A double seismic zone in the subducting Juan Fernandez Ridge of the Nazca Plate (32°S), central Chile,. Journal of Geophysical Research : Solid Earth, 2013, 118 (7), pp.3462-3475. 10.1002/jgrb.50240 . hal-00932805

HAL Id: hal-00932805
https://hal.science/hal-00932805

Submitted on 10 Nov 2021

HAL is a multi-disciplinary open access archive for the deposit and dissemination of scientific research documents, whether they are published or not. The documents may come from teaching and research institutions in France or abroad, or from public or private research centers.

L'archive ouverte pluridisciplinaire **HAL**, est destinée au dépôt et à la diffusion de documents scientifiques de niveau recherche, publiés ou non, émanant des établissements d'enseignement et de recherche français ou étrangers, des laboratoires publics ou privés.

Copyright

A double seismic zone in the subducting Juan Fernandez Ridge of the Nazca Plate (32°S), central Chile

M. Marot,[1] T. Monfret,[1] M. Pardo,[2] G. Ranalli,[3] and G. Nolet[1]

Received 8 January 2013; revised 31 May 2013; accepted 5 June 2013; published 8 July 2013.

[1] The region of central Chile offers a unique opportunity to study the links between the subducting Juan Fernandez Ridge, the flat slab, the double seismic zone (DSZ), and the absence of modern volcanism. Here we report the presence and characteristics of the first observed DSZ within the intermediate-depth Nazca slab using two temporary seismic catalogs (Ovalle 1999 and Chile Argentina Seismological Measurement Experiment). The lower plane of seismicity (LP) is located 20–25 km below the upper plane, begins at 50 km depth, and merges with the lower plane at 120 km depth, where the slab becomes horizontal. Focal mechanism analysis and stress tensor calculations indicate that the slab's state of stress is dominantly controlled by plate convergence and overriding crust thickness: Above 60–70 km depth, the slab is in horizontal compression, and below, it is in horizontal extension, parallel to plate convergence, which can be accounted for by vertical loading of the overriding lithosphere. Focal mechanisms below 60–70 km depth are strongly correlated with offshore outer rise bend faults, suggesting the reactivation of preexisting faults below this depth. The large interplane distances for all Nazca DSZs can be related to the slab's unusually cold thermal structure with respect to its age. Since LPs globally seem to mimic mantle mineral dehydration paths, we suggest that fluid migration and dehydration embrittlement provide the mechanism necessary to weaken the rock and that the stress field determines the direction of rupture.

Citation: Marot, M., T. Monfret, M. Pardo, G. Ranalli, and G. Nolet (2013), A double seismic zone in the subducting Juan Fernandez Ridge of the Nazca Plate (32˚S), central Chile, *J. Geophys. Res. Solid Earth*, *118*, 3462–3475, doi:10.1002/jgrb.50240.

1. Introduction

[2] In central Chile, the Nazca Plate and Juan Fernandez Ridge subduct beneath the South American continental lithosphere. Two temporary local seismic campaigns were carried out over central Chile-western Argentina (29°S–34°S) and enabled the detection of a double seismic zone (DSZ) in the region (Figure 1). The DSZ is most noticeable along the Juan Fernandez Ridge (JFR) track, an aseismic volcanic chain subducting beneath South America. This DSZ was first mentioned by *Pardo et al*. [2004].

[3] DSZs consist of two planes of seismicity, more or less parallel to one another, located within the subducting oceanic slab at intermediate depths (50–200 km). An exception is *McGuire and Wiens*'s [1995] apparent recognition of one at ~600 km of depth within the Tonga slab. In all cases, the upper seismic plane (UP) locates within or near the oceanic crust, as verified by seismic tomography, while the lower seismic plane (LP) locates at variable depths within the oceanic mantle. The planes are separated by a region of reduced seismicity. They are observed at least once in every subduction zone and are therefore suggested as ubiquitous features of subduction zones [*Brudzinski et al*., 2007]. The first and best occurrence of a DSZ and also the much rarer triple seismic zone are found in the Pacific slab beneath northern Honshu, Japan, with 30–40 km and ~10 km of separation distances between the planes, respectively [*Hasegawa et al*., 1978; *Seno and Pongsawat*, 1981; *Kawakatsu and Seno*, 1983].

[4] Recent improvements in station coverage and data processing tools have enabled DSZs to be increasingly and more accurately detected, with separation distances as small as 9 km, such as in northern Chile [*Rietbrock and Waldhauser*, 2004]. Previous studies also suggest their presence when layers of different focal mechanisms are observed [e.g., *Comte and Suárez*, 1994]. However, hypocentral locations have uncertainties that sometimes are larger than the suggested separation between UP and LP, rendering their recognition and measurement difficult. A list of global DSZ occurrences and their reported characteristics is shown in Table 1.

[5] There are a few global characteristics common to all DSZs that can be recognized: (i) LPs begin beneath the plate interface at ~50 km depth; (ii) UPs and LPs usually merge between 100 and 150 km depth; and (iii) UPs are composed of more events with smaller magnitudes than LPs [*Fujita*

[1]GéoAzur, UNSA, CNRS, OCA, Valbonne, France.
[2]Departamento de Geofisica, Universidad de Chile, Santiago, Chile.
[3]Department of Earth Sciences, Carleton University, Ottawa, Ontario, Canada.

Corresponding author: M. Marot, GéoAzur, Bât 1, 250 rue Albert Einstein, Les Lucioles 1, Sophia Antipolis, FR-06560 Valbonne, France. (marot@geoazur.unice.fr)

©2013. American Geophysical Union. All Rights Reserved.
2169-9313/13/10.1002/jgrb.50240

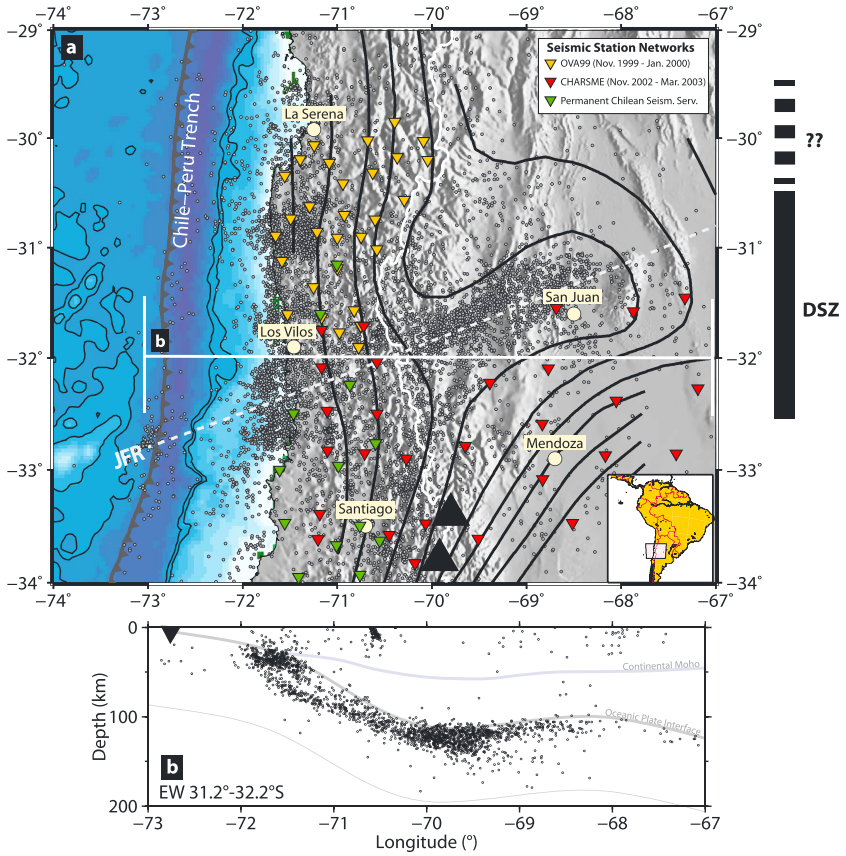

Figure 1. Regional seismic context. (a) Plan view: Yellow and red inverted triangles represent the OVA99 and CHARSME temporary seismic station network, respectively; circles are the recorded seismicity. Dashed white line indicates the subduction track of the Juan Fernandez Ridge (JFR). Solid lines are isodepth contours (every 20 km) featuring the shape of the slab's surface [*Anderson et al.*, 2007]. Black triangles denote the location of active volcanoes. Thick solid and dashed black lines, on the right, indicate the latitudes where the DSZ is clearly observed and where it is questionable, respectively. (b) Vertical profile of the seismicity between 31.2°S and 32.2°S, where the double seismic zone (DSZ) is well observed. Hypocenter uncertainty here is 15 km in all directions. Inverted black triangle locates the trench axis, and solid gray lines indicate the positions of continental Moho [*Fromm et al.*, 2004], slab surface [*Tassara and Echaurren*, 2012], and modeled Lithosphere-Asthenosphere Boundary (LAB) [*Tassara et al.*, 2006].

and Kanamori, 1981]. An attempt to classify DSZs into three classes according to their focal mechanism distributions was made by *Kao and Rau* [1999]: (i) "Type I": compression along UPs and tension along LPs (e.g., Japan, Kurile); (ii) "Type II": tensional UPs and compressional LPs (e.g., beneath southern North Island in New Zealand, north of the Cape Mendocino Triple Junction in Cascadia, and Cook Inlet in Alaska); and (iii) "Type III": lateral compression in the shallowest part of the DSZ (due to plate convergence) and downdip tension in the deeper part (due to slab pull) (e.g., Philippine Sea plate beneath Taiwan).

[6] Earthquakes reflect the state of stress of the lithosphere. A subducting plate accumulates stress via several mechanisms: plate interaction, slab pull, mantle viscous drag, thermal stresses, slab bending and unbending, and basalt-eclogite transformations in the crust [*Fry et al.*, 2009]. These are in turn influenced by convergence rate, subduction angle, slab age, subduction rollback, mantle viscosity structure, and deeper mantle phase transitions [*Fry et al.*, 2009]. *Brudzinski et al.* [2007] described a positive correlation between separation distances in seismic planes in DSZs and slab ages from global observations. This, however, does not match our data, which show a larger separation distance. What controls DSZ global occurrence, widths, depth limits, tendencies for merging at depth, and stress distribution is still a subject of debate.

[7] Here we describe the central Chilean DSZ, with an interplane distance of 20–25 km, in terms of its seismic distribution, focal mechanism solutions, and *P* and *T* axes orientations, as well as our stress tensor calculations for the UP and LP, in order to better understand the DSZ's occurrence and origin in this region's complex subduction dynamics. We assess the influence of the varying slab geometry and the subducting JFR on the occurrence of the DSZ and consider possible controlling mechanisms. We also compare our observations with other known DSZs in the Nazca slab and worldwide and conclude that the Central Chilean DSZ is a rare "type III" case, where both seismic planes are affected by the same stress regime, which, however, change at a critical depth. This observation also enables us to rule out plate bending or sagging

Table 1. Global Double Seismic Zone (DSZ) Observations[a]

Locality	Plate Age (Ma)	Starting Depth (km)	End Depth (km)	Width (km)	UP Stress	LP Stress	Reference
Northeast Japan Northern Honshu-Hakkaido	133	50	160	30–40	C	T	*Hasegawa et al.* [1978]
Southwest Japan Kanto	133	50	75	20	C	T	*Seno et al.* [2001]
Northeast Taiwan Ruyku Trench	45	40–50	150	10–20	C	C	*Kao and Rau* [1999]
Northern Chile (18.5°S–19.5°S)	47	80	150	20–25	Mixed	Mixed	*Comte et al.* [1999]; *Dorbath et al.* [2008]
Northern Chile (20°S–24°S)	43	80	150	15	T	C	*Comte and Suárez* [1994]
Northern Chile (22°S)	43	80	130	9	T	T	*Rietbrock and Waldhauser* [2004]
Central Chile (30°S–32°S)	35	50	100–120	30	T	T	This study
Cape Mendocino Cascadia Trench	10	15	25	9	T	C	*Wang and Rogers* [1994]
Eastern Aleutian Shumagin Islands	50	70	175	30–40	Mixed	Mixed	*Ratchkovsky et al.* [1997]
Central Aleutians	56	100	175	25	C	T	*Engdahl and Scholz* [1977]
New Zealand Wellington Region	90	50	80–90	20	T	C	*Robinson* [1986]
Kurile-Kamchatka	125	50	170–180	40	C	T	*Kao and Chen* [1994]
New Britain	130	60	170	15	C	T	*McGuire and Wiens* [1995]
New Hebrides Vanuatu Trench	84	10–40	80	50–70	C	T	*Prevot et al.* [1994]
Northern Marianas (17°N–19°N)	170	60	180	30	C	T	*Shiobara et al.* [2010]

[a]Plate ages at the trench are estimated from digital isochron measurements [*Müller et al.*, 1997]. Also shown are starting and finishing depths of the lower seismic planes, maximum separation distances (width) between seismic planes, and stress regimes inferred from focal mechanisms (T: tension, C: compression).

as a possible mechanism for the DSZ. Finally, our focal mechanisms indicate that subducted outer rise faults become dominantly reactivated below 60–70 km depth.

2. Regional Context

[8] Below central Chile and western Argentina (29°S–34°S), the Nazca Plate subducts beneath the South American plate at a convergence rate of 6.7 ± 0.2 cm/a in the N78° direction as constrained by GPS measurements [*Kendrick et al.*, 2003]. The slab age at the trench is 33–38 Ma [*Clouard et al.*, 2007]. High plate convergence and strong plate coupling are characteristic of the region and result in back-arc compression and trench retreat [*Heuret and Lallemand*, 2005; *Heuret et al.*, 2007; *Lallemand et al.*, 2008]. Continental crustal thickness reaches 70 km below the Principal Cordillera and 55 km below the Sierras Pampeanas (Figure 1b) [*Gilbert et al.*, 2006; *Heit et al.*, 2008, *Tassara and Echaurren*, 2012].

[9] The slab geometry exhibits the world best observed 250 km-long ("Pampean") flat slab segment [*Isacks and Barazangi*, 1977; *Ramos et al.*, 2002; *Pardo et al.*, 2004]. The Nazca slab initially subducts everywhere along the Peru-Chile Trench at ~25°–30° dip, until 100 km of depth where, in central Chile between 27°S–32.5°S, it becomes horizontal and underplates the overriding lithosphere [*Barazangi and Isacks*, 1976; *Cahill and Isacks*, 1992; *Araujo and Suárez*, 1994; *Pardo et al.*, 2002; *Ramos et al.*, 2002]. The Pampean flat slab is bounded to the south by a sharp transition zone (>32.5°S) whereby the slab dip returns to normal (~30°) over a short distance, with a yet unconstrained along-strike mode of deformation (rupture versus flexure). *Smalley and Isacks* [1987] used data from the local permanent Argentinean network Instituto Nacional de Prevencion Sismica (INPRES) to observe a flexure rather than a tear at depth <125 km. This conclusion was later supported by *Araujo and Suárez* [1994] using teleseismic focal mechanisms and recently by *Pesicek et al.* [2012] from a tomographic model of the mantle. The northern transition zone (~27°S) is broader and gentler [*Cahill and Isacks*, 1992; *Pardo et al.*, 2002; *Anderson et al.*, 2007].

[10] The causes for slab flattening are yet unclear. However, there appears to be a strong influence from the subducting Juan Fernandez Ridge (JFR) track, which should provide extra buoyancy to the already young slab. Similarly, the Peruvian flat slab segment is also correlated to the extensive Nazca Ridge plateau. In both cases, the flat slab segments are reflected on the surface by an absence of Quaternary arc volcanism and, in the case of the Pampean flat slab, also by a narrowing of the central Chilean valley for the past 9–10 Ma [*Barazangi and Isacks*, 1976; *Jordan et al.*, 1983; *Kay et al.*, 1987; *Yáñez et al.*, 2002].

[11] The JFR subduction track is characterized by dense microseismicity ($M_w < 5$) (Figure 1). The JFR is a volcanic seamount chain showing a linear increase in age inferred from magnetic anomalies. It is observed by global seismic tomography as originating from a narrow deep-seated mantle plume extruding at 97.5°W and 34°S [*Montelli et al.*, 2004; *Kopp et al.*, 2004, *Zhao*, 2007]. It extends 900 km on the seafloor, in ~EW direction, and enters the Chilean trench near normally at 32.5°S, subducting beneath the overriding continental plate.

[12] The ridge migrated southward along the Peru-Chile Trench over the past 22 Ma to its current location [*Yáñez et al.*, 2002]. Its interaction with the overriding plate resulted in marginal erosion, shoreline indentation, crustal uplift and thickening on the continental side [*Fromm et al.*, 2004], and a seaward shift in outer rise events on the oceanic side [*Clouard et al.*, 2007]. It also participated in the formation of a sediment barrier at 32.5°S, with a sediment-poor trench to the north and a sediment-rich trench to the south, lasting since ~16 Ma [*Lowrie and Hey*, 1981], as well as probably provoking the change of slab geometry in conjunction with the high overriding plate trenchward motion [*Pilger*, 1981; *Cahill and Isacks*, 1992; *Ramos et al.*, 2002; *Yáñez et al.*, 2002; *Martinod et al.*, 2005; 2010]. Hence, the interaction of this feature with the continental plate generates important disturbances despite its moderate size. Since the central Chilean DSZ is observed within and around the subducting

JFR track, understanding whether a relationship exists between them could provide additional insight on the mechanisms that control the double-planed seismicity pattern inside a subducting slab (e.g., mechanical and compositional controls).

3. Data Analysis and Results

[13] The regional seismicity was recorded by the two temporary seismic campaigns OVA99 (Ovalle 1999) and CHARSME (Chile Argentina Seismological Measurement Experiment) in central Chile and western Argentina (Figure 1a). Both networks were installed and maintained by a collaborative group from GéoAzur laboratory, France, and the Departamento de Geofísica of the University of Chile. For the CHARSME campaign, the collaboration of the University of San Juan and logistical support of INPRES in Argentina were also available.

[14] The OVA99 seismic network was deployed in the region of Ovalle (30°S–32°S, 72°W–70°W) in central Chile during the period mid-November 1999 to mid-January 2000. Thirty-seven short-period three-component receivers (2 Hz and 4.5 Hz), about 30 km apart, recorded continuously the local microseismicity ($0.5 < M_l < 5.5$) with a sampling rate of 125 sps.

[15] The CHARSME campaign was carried out from mid-November 2002 to March 2003 for the purpose of analyzing the regional seismotectonic features and to map the shift in subduction geometry of the Nazca slab. It comprised 29 portable broadband three-component stations (27 CMG-40 T and two CMG-3 T Guralp) that continuously recorded seismicity with a sampling rate of 125 sps. In an effort to increase station coverage and improve hypocenter determination, particularly near coastal areas, 15 permanent seismic stations (short period and broadband) from the Chilean Seismological Service of the University of Chile were also used (Figure 1a).

3.1. Hypocenter Location

[16] Hypocenter location was performed by manual picking of first arrivals of *P* and *S* waves [*Pardo et al*., 2004]. Initial velocity models were calculated from mining blasts for the first 20 km of depth and using the VELEST (a program designed to derive 1-D velocity models for earthquake location techniques and as initial reference models for seismic tomography methods; its current name was given by R. Nowack) algorithm [*Kissling et al*., 1994] for larger depths. The average 1-D velocity model of least square fit that best describes the arrival times is a 17-layer model with Vp/Vs of 1.76. Local magnitudes (M_l) were calculated (Figure 2) for all events, accounting for maximum amplitude and hypocentral distance [*Lay and Wallace*, 1995], and calibrated such that the M_l values remain close to the M_w values available from the International Seismological Centre (ISC) catalog [*Marot et al*., 2012].

[17] Only the most reliable events were selected with strict criteria: (i) In Figure 1b, we show only events with maximum hypocenter uncertainties of 10 km in horizontal coordinates and 5 km in depth; and (ii) in Figure 3, we further restrict the selection to minimum 10 seismic phases including at least two *S* phases and maximum RMS misfit ($\sqrt{\Sigma R_i^2}/N$ where R_i is the time residual at the *i*th station) ≤0.6 s. The DSZ is more noticeable when all the recorded seismicity is shown, indicating that even the events deemed "unreliable" due to too few phase pickings concentrate along the seismic planes, emphasizing the accuracy of the DSZ's inferred geometry. Nevertheless, we chose to show only the most accurately determined events (Figure 3). Also, we have performed the relative earthquake relocation method *HypoDD* [*Waldhauser and Ellsworth*, 2000] and found it inconclusive, with no significant difference with the initial hypocenter locations. Therefore, we deemed sufficient to show the earthquake distribution obtained with the classical location method.

[18] The DSZ clearly occurs between latitudes 30.5°S and 32.5°S (Figure 1b) and may also be present between 29.5°S and 30.5°S, where station coverage is lacking (Figure 3i). However, where station coverage is adequate at ~33°S, we have difficulty attesting its presence (Figure 3iv).

[19] Where we observe it clearly, the LP begins below the plate interface at 50 km of depth, as in other case studies (Table 1). Some events also locate below the trench axis at depths ~25–40 km (Figures 1b and 3), possibly forming the western extension of the LP within the slab. The LP has a slightly higher seismic activity than the UP and extends downward until merging with the UP at ~100–120 km of depth, where the slab bends upward into horizontal subduction. The maximum interplane distance, as measured by the perpendicular distance between the two peaks in seismic activity, is 20–25 km beneath the plate interface. The magnitude distributions and standard deviations are similar along the UP and LP with an average M_l of 2.3 (±0.9) and 2.4 (±0.6), respectively (Figures 2b and 2c).

3.2. Focal Mechanisms

[20] Equal-area projections of earthquake double-couple focal mechanisms were obtained from first *P* wave polarities using program focal mechanism determinations (FOCMEC) (seismic analysis, or SEISAN, an earthquake analysis software package; *Snoke et al*. [1984]) for the earthquakes that meet the selection criteria. In total, 1065 focal mechanisms were calculated for the entire region. *Pardo et al*. [2004] used these results to infer the slab's state of stress at different depth intervals but did not account for the DSZ. We show DSZ focal mechanisms across a 100 km-wide profile between 31.2°S and 32.2°S (Figure 4), where the slab geometry is constant and seismic density is highest. To increase accuracy and reliability of our results, we visually assessed every first *P* wave arrival and polarity reading and determined nodal planes based on a minimum of nine polarity readings allowing 1–5° increment of solution variation. We obtained 13 and 23 reliable focal solutions for the UP and LP, respectively (Table 2).

[21] Both seismic planes indicate the same variations in normal and reverse focal mechanisms, with a clear dominant extensional faulting trend: (i) UP: 70% normal faulting, 30% reverse faulting and (ii) LP: 80% normal faulting, ~20% reverse faulting. Contrary to most global observations for DSZs, there appears to be no partition in focal mechanism type between the seismic planes of the central Chilean DSZ (compare with Table 1).

[22] However, a partitioning with depth can be noticed between normal and reverse focal mechanisms (Figure 4b). Although a strong strike-slip component is pervasive at any depth, events with reverse mechanisms tend to be separated

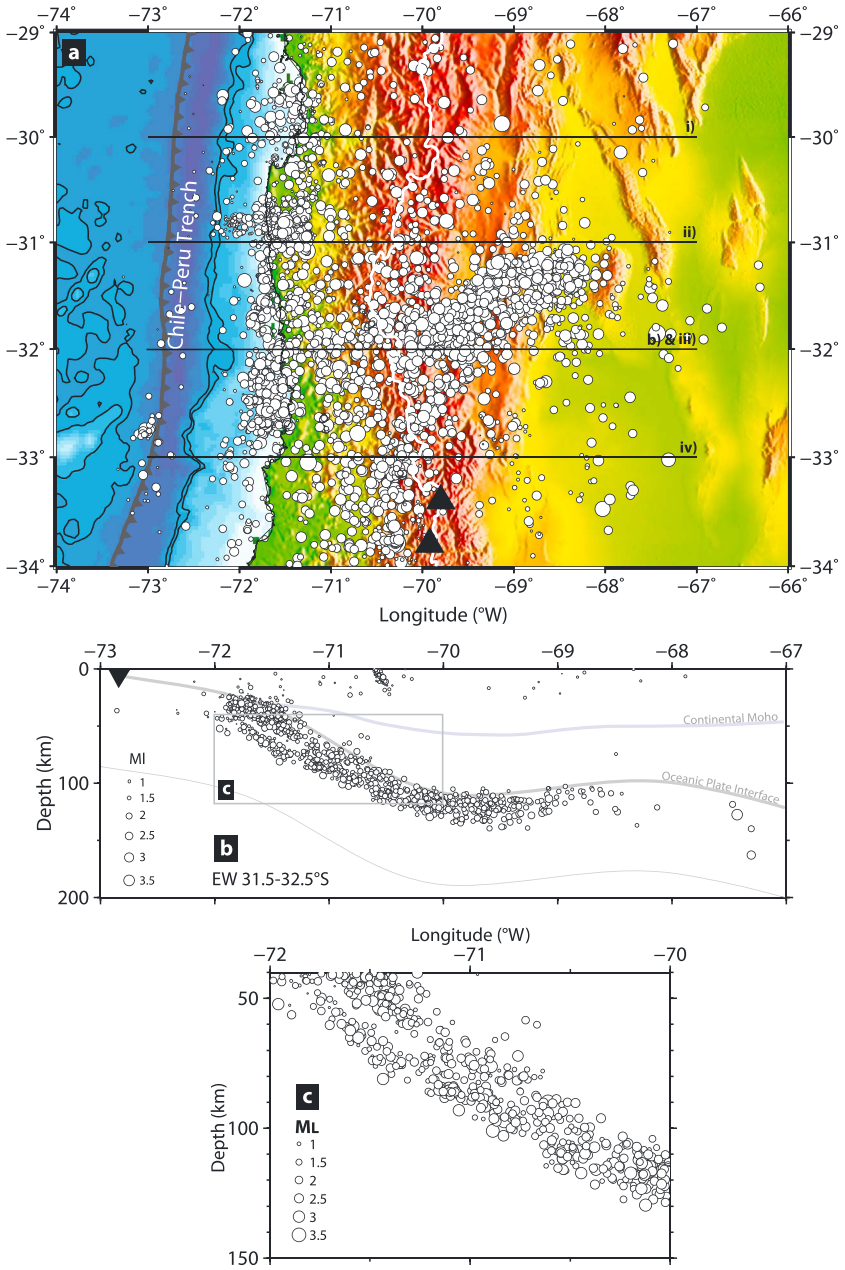

Figure 2. Earthquakes (circles) scaled on the basis of their local magnitude. (a) Plan view. Horizontal lines, i) to iv), refer to the vertical profiles in Figure 3. (b) Vertical profile (also shown in Figure 3, profile iii). Refer to legend in Figure 1. (c) Close-up of the DSZ's seismicity and magnitude distribution.

from normal mechanisms at the 60–70 km depth limit, with normal mechanisms occurring almost exclusively below this limit. Focal solutions above this depth show no particular strike pattern but tend to have dip angles of 60°E (Figure 4c). Below this depth, a remarkable change in strike pattern occurs, strongly trending NS, parallel to the trench axis, and dipping 40°W, indicating a dip angle of ~70° from the slab surface.

3.3. *P* and *T* axes

[23] The discrepancy between the types of focal mechanisms at the 60–70 km depth limit can be observed also from the variations in azimuth and plunge orientations of the *P* and *T* axes (Figure 5). Above 60–70 km, *P* axes strike mainly with an EW component and a slabdip plunge oscillating between 0°E and 30°E (Figure 5a). Below 60–70 km, their strike is variable with subvertical predominant plunge angles between 60° and 90° (Figure 5b). On the contrary, *T* axes above 60–70 km have variable strikes with essentially high plunge angles between 60° and 80° (Figure 5a), while below 60–70 km they have a well-defined EW strike tendency, similar to *P* axes above 60–70 km (Figure 5a), with slabdip plunge angles between 0°E and 30°E (Figure 5b). *Anderson et al.* [2007] demonstrated, using local earthquake focal mechanisms, that *T* axes along the flat slab are subhorizontal but trend normal to the directions of subduction and the JFR track. This shows that the slab is being stretched sideways as a consequence of the slab's kinematics. In addition, they

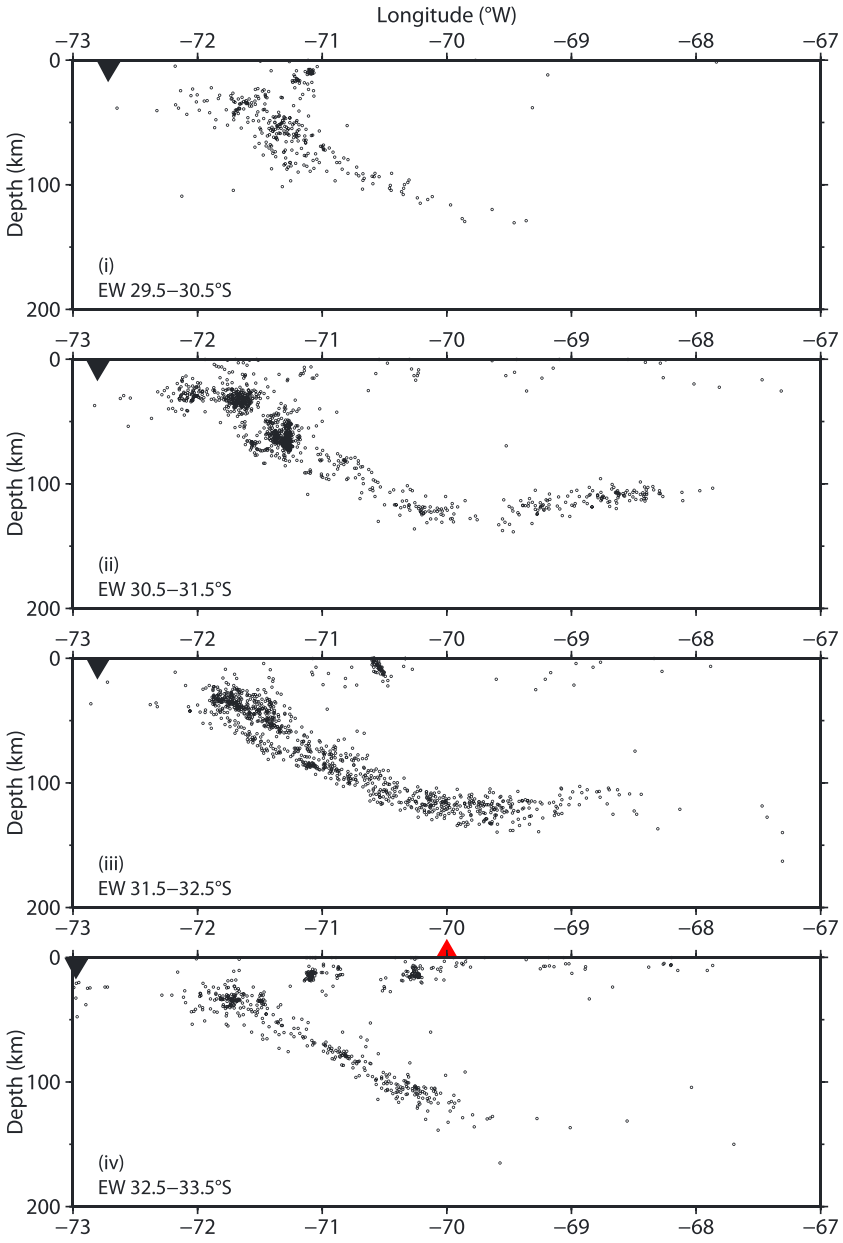

Figure 3. EW vertical cross sections of the earthquake distribution (see Figure 2 for locations), illustrating the NS extent of the DSZ (also shown in Figure 1). Hypocenter uncertainty here is 5 km in the vertical and 10 km in the horizontal direction, respectively. Inverted black triangles and red triangle show the trench axis and active volcanoes, respectively.

show that *P* axes are subhorizontal and parallel to the direction of subduction and the JFR path. These strong differences in *P* and *T* axes orientations between the flat slab and the DSZ suggest that, despite their proximity, they are not influenced by the same tectonic regime. The slab is in slabdip compression down to 60–70 km depth, in slabdip extension between 60–70 km and 100–120 km depth, and in slabdip compression but laterally stretched along the flat part.

3.4. Stress Tensor

[24] The stress tensor was calculated based on the code developed by Delouis [*Delouis et al*., 2002]. Considering the average scalar product of the differences between the slip vectors, determined by the focal mechanisms, and those predicted by the stress tensors, our solutions are presented in Figure 6 at three levels of confidence: (1) the best fitting model (the highest score) denoted by colored circles, (2) the second best solutions (gray circles), situated between the best score and 97% of the best score, and (3) the third best solutions (white circles), situated between 94% and 97% of the best score. Initially, we attempted to find a stress tensor accounting for the UP and LP separately, as is commonly shown in other studies. This attempt generated a poorly constrained solution with low scores (UP: 63%; LP: 59%). This suggests that there are perhaps insufficient data to well constrain the solution or that the central Chilean DSZ seismicity is not dominated by a stress regime such as bending/unbending, which would tend to dissociate the seismic planes

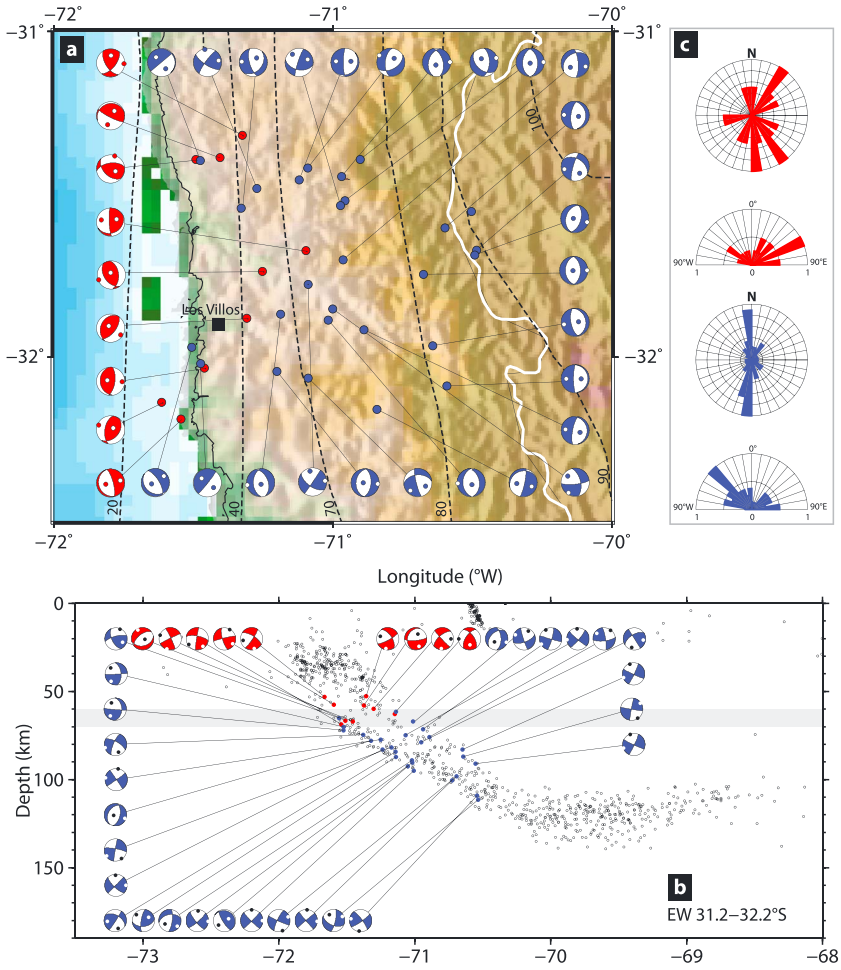

Figure 4. Focal mechanism solutions along profile 31.2°S–32.2°S (also shown in Figure 1b). (a) Plan view: Red and blue focal mechanisms represent those above and below the depth limit of 60–70 km, respectively. Dotted lines indicate the isodepth contours. Thick white line is the political border between Chile and Argentina. (b) Vertical profile: Color code as in Figure 4a. Thick gray line shows the 60–70 km depth limit. (c) Strike and dip rose diagrams of the focal mechanism solutions with focal depth < 60–70 km (red) and >60–70 km (blue).

into two separate stress regimes (e.g., numerous examples in the Pacific slab; Table 1).

[25] The focal mechanisms that do not fit well the models for the UP and LP are located in the 60–70 km depth range. We also calculated stress tensors for the UP and LP above and below 60–70 km depth ("UP < 60–70 km," "UP > 60–70 km," "LP < 60–70 km," and "LP > 60–70 km" in Figure 6). The only solutions that give good results (best score > 95%) are those for the UP > 60–70 km and the LP < 60–70 km. However, a constraint on these results lies in the few data used in each group, particularly for UP > 60–70 km. Since stress tensor solutions for above 60–70 km of depth are similar for the two planes, regardless of their score, and likewise for those below 60–70 km, we chose to group them together in the two depth ranges. Because we find both types of focal mechanisms between 60 and 70 km, in order to identify which group they belong to, we incorporated them individually into our stress tensor calculations and verified that a good fit was maintained. Although we are restricted to a number of nine focal mechanisms for above 60–70 km and 18 for below 60–70 km, we obtained two coherent and well-constrained stress tensor solutions for this area (Figure 6).

[26] Our preferred stress tensor solution for the central Chilean DSZ is the one shown in Figure 6. In both cases (above and below 60–70 km of depth), the σ_3 axis is very well determined, with azimuth consistently parallel to direction of convergence (78°N) and plunging subvertically above 60–70 km depth and subhorizontally below 60–70 km depth. The solutions for the σ_1 and σ_2 axes for both above and below 60–70 km depth indicate that they are interchangeable, reflecting heterogeneity in the main acting forces in the region. However, if we consider only the best fitting models with the best scores for each case (colored dot in Figure 6), we observe the following: (i) above 60–70 km of depth, σ_1 is subhorizontal, and σ_3 is subvertical, both trending parallel to the direction of convergence with a shape factor of −1.41, which indicates predominant reverse faulting [*Rivera and Cisternas*, 1990]. The σ_2 axis is horizontal and oriented NS. This solution of convergence-parallel compression is in good agreement with the region's tectonic context of high convergence rate and degree of interplate coupling. Furthermore,

Table 2. Focal Mechanism Solutions Obtained for the Profile 31.2°S–32.2°S[a]

	Longitude (deg)	Latitude (deg)	Z (km)	M_l	Strike1 (deg)	Dip1 (deg)	Rake1 (deg)	Strike2 (deg)	Dip2 (deg)	Rake2 (deg)
1[b]	−71.375	−31.319	57.8	2.2	251	14	45	117	80	100
2[b]	−71.302	−31.737	59.8	2.9	145	47	69	354	47	111
3[b]	−71.147	−31.674	62.8	1.5	148	60	35	39	60	145
4[b]	−71.358	−31.881	52.5	1.0	206	30	80	38	61	96
5	−71.510	−32.033	66.5	2.7	174	26	78	7	65	96
6	−71.595	−32.189	57.5	1.6	345	75	−89	161	15	−94
7	−71.664	−32.138	52.9	2.2	190	56	72	40	38	115
8	−71.541	−31.394	68.6	1.5	177	81	70	64	22	155
9	−71.455	−31.388	67.0	2.4	262	56	53	135	49	132
10[b]	−70.952	−31.394	78.7	3.0	1	58	−60	134	43	−1
11[b]	−71.375	−31.319	57.8	2.2	251	14	45	12	81	−105
12[b]	−71.067	−31.887	74.8	1.7	193	51	−76	351	41	−107
13[b]	−70.938	−31.916	71.4	1.2	191	75	−84	349	16	−111
14[b]	−70.642	−32.088	87.0	1.5	180	80	−89	354	10	−96
15[b]	−70.553	−31.554	91.0	1.3	187	65	−84	353	26	−103
16[b]	−70.648	−31.604	83.0	1.5	187	65	−84	353	26	−103
17	−70.725	−31.747	100.5	1.9	180	40	−89	359	50	−91
18	−70.692	−31.965	98.1	1.9	350	25	−89	169	65	−90
19	−71.138	−32.064	87.2	3.2	166	81	−46	265	45	−167
20	−71.238	−31.868	82.9	2.5	180	46	−75	339	46	−105
21	−71.051	−31.852	92.4	2.9	346	59	−15	84	77	−148
22	−70.534	−31.673	111.5	2.8	196	78	−50	300	41	−162
23	−70.541	−31.687	109.1	2.8	196	36	−89	15	54	−91
24	−71.524	−32.020	70.1	2.9	218	4	90	38	86	90
25	−71.525	−31.397	71.9	3.1	50	90	84	320	6	180
26	−71.251	−32.044	77.2	1.9	185	35	−89	4	55	−91
27	−71.374	−31.544	74.6	1.7	39	35	−41	164	68	−118
28	−71.019	−31.446	90.4	1.9	196	42	−66	345	52	−110
29	−71.323	−31.483	77.9	1.5	216	80	18	123	72	169
30	−71.006	−31.521	95.0	1.0	185	45	−82	354	46	−98
31	−71.140	−31.420	84.3	1.3	60	48	−47	186	57	−127
32	−71.022	−31.536	89.0	1.8	198	83	45	101	45	170
33	−71.171	−31.457	81.8	1.6	47	14	−44	180	80	−100
34[b]	−71.014	−31.702	67.0	2.2	235	32	−35	356	72	−117
35[b]	−71.139	−31.777	61.4	1.2	34	88	−29	125	61	−178
36	−71.556	−31.970	65.0	3.1	328	68	−83	130	23	−107

[a]Focal mechanisms 1–9 refer to events above 65 km of depth (red beach balls in Figure 4) and 10–36 to those below this depth (blue beach balls in Figure 4).
[b]UP events.

similar stress tensor solutions were obtained for the back-arc crust (Figure 7) [*Pardo et al*., 2002; *Alvarado et al*., 2005]. (ii) Below 60–70 km of depth, the σ_1 axis is subvertical and σ_3 is subhorizontal trending parallel to the direction of convergence, and the shape factor indicates predominant normal faulting (1.13). The σ_2 axis is identical to that above 60–70 km depth. This suggests that the slab is in subhorizontal extension below 60–70 km depth. These results are in agreement with *Pardo et al*. [2002] and *Salazar* [2005] results for this region.

4. Discussion

[27] In this work, we present evidence for a DSZ in central Chile with an interplane distance of 20–25 km. The LP is best identified between latitudes ~30.5°S and 32.5°S, coincident with the location of the JFR subduction track, where seismic activity is highest, but is still noticeable at latitude 29.5°S, amounting to a total trench-parallel length of ~300 km. The uneven seismic coverage of the region renders its relationship with the JFR unclear. Nevertheless, if we consider the width proposed by *Kopp et al*. [2004] and assume that it remains constant with depth, the DSZ is found in a geographical range that is broader than the JFR track, suggesting that it is perhaps not directly related to the JFR properties.

[28] Our observation of the DSZ ends at ~32.5°S, close to the southern transition zone, where good station coverage existed during our data recording but seismic rate falls. This means that either it exists further south but is concealed by low seismicity, or it is truly nonexistent due to local factors causing the reduction in seismicity and the LP to vanish. Other seismic studies southward of our region [e.g., *Campos et al*., 2002; *Haberland et al*., 2009] have not reported any DSZ. Since the geographical extent of the central Chilean DSZ appears to be constrained by the regions bounding the flat slab, one can suppose that it is affected by changes in slab geometry. Indeed, the return to normal subduction creates increased slab stresses due to localized lateral deformations, as demonstrated by *Anderson et al*., [2007], and changes in the system's thermal state, as hot asthenosphere is reintroduced into the corner wedge [*Wada and Wang*, 2009; *Syracuse et al*., 2010], a process witnessed by the return of active volcanism at the surface. Therefore, we expect the contrast in slab temperature and rheology that arises between flat and normal subduction regions to affect the viability of the central Chilean DSZ, particularly along its more abrupt southern margin.

[29] Within the Nazca slab, two other DSZs have been reported to date, both in northern Chile. They are located side by side, one at 18.5°S–19.5°S [*Comte et al*., 1999; *Dorbath et al*., 2008] and the other at 20°S–24°S [*Comte and*

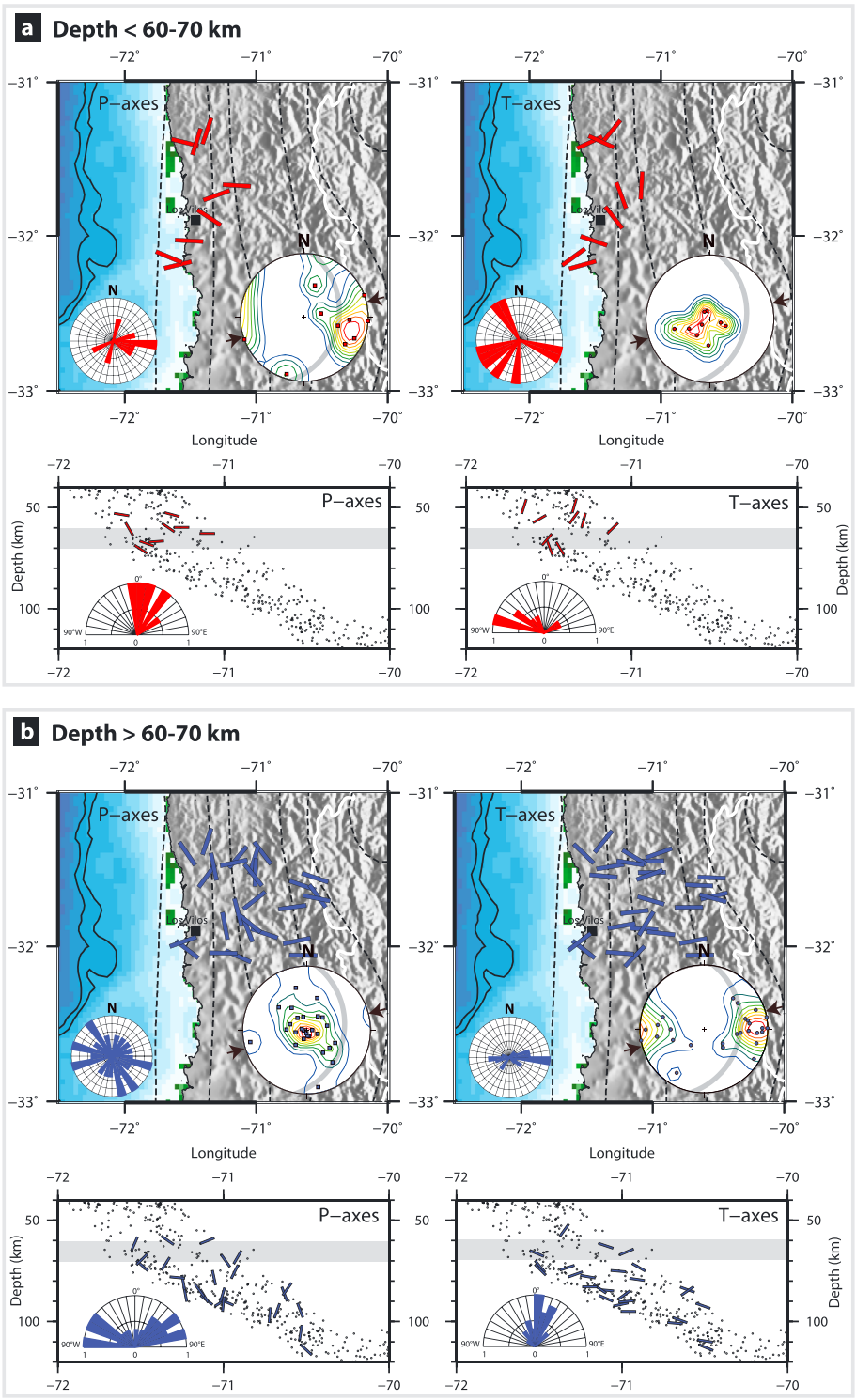

Figure 5. Strike and dip orientations of *P* and *T* axes, determined from the focal mechanisms at (a) <60–70 km depth (red), and (b) >60–70 km (blue). The strike and dip orientations are shown by (1) stereonet representations, as lower hemisphere projections, with the slab orientation shown by the thick gray great circle at the DSZ's depth, (2) rose diagrams, and (3) EW vertical profiles of the dip angles, projected in the EW direction in order to show the relation with the slab dip.

Suárez, 1994; *Rietbrock and Waldhauser*, 2004]. They exhibit two different stress patterns and interplane distances (see Table 1). This rapid change in DSZ characteristics along strike suggests that they reflect changes in ambient stresses and are complex features of slabs that do not necessarily connect smoothly with one another.

[30] Several other studies of global DSZs recognized their sensitivity to slab age, particularly in regard to their

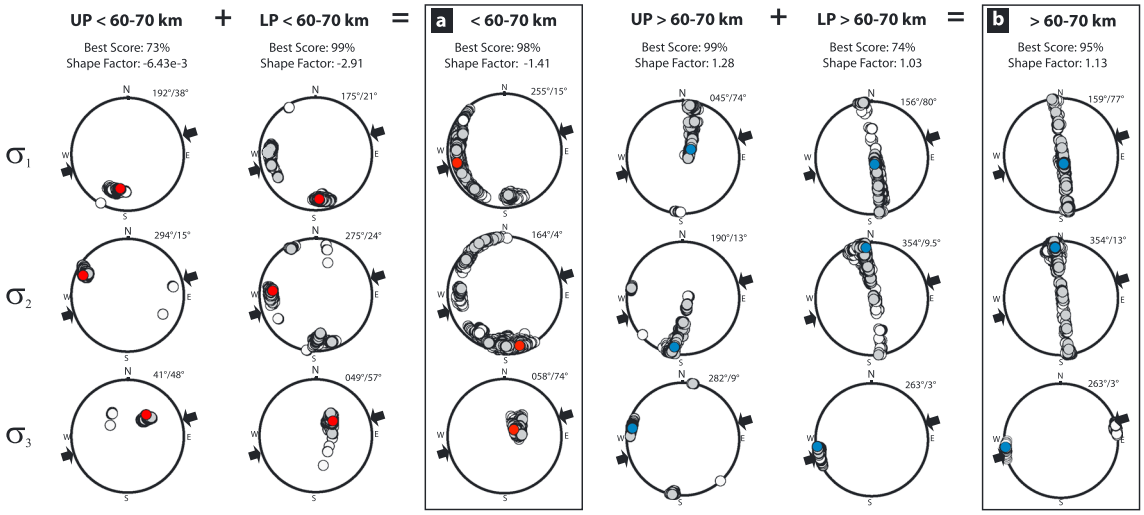

Figure 6. Stress tensor solutions (σ_1, σ_2, σ_3 axes, azimuth/plunge orientations, best score, and shape factor) projected on lower hemispheres, calculated for the focal mechanisms shown in Table 2 and Figure 4. Black arrows indicate the direction of convergence of Nazca Plate. The best solutions (best score) are indicated by red (<60–70 km depth) and blue (>60–70 km depth) circles. All other solutions found at levels >97% and >94% of the best score are shown in gray and white circles, respectively. Our selected stress tensors for the region above and below the 60–70 km depth limit, and used for our interpretation, are shown in Figures 6a and 6b, respectively. A shape factor <0 corresponds to a compressional regime, between 0 and 1 to a strike-slip regime, and >1, to an extensional regime [*Rivera and Cisternas*, 1990].

interplane distances. The interplane distance observed for the central Chilean DSZ is 20–25 km and is unexpectedly large compared to *Brudzinski et al.*'s [2007] estimate of 0.14 km/Ma, deduced from global earthquake catalog Engdahl, van der Hilst and Buland (EHB) earthquake catalog [*Engdahl et al.*, 1998]. The central Chilean DSZ could not be detected using this database, because of the region's too dense seismicity. According to *Brudzinski et al.* [2007], a plate of age of ~40 Ma, as in our case, should correspond to an interplane distance of ~6 km and not 20–25 km. The same discrepancy applies for northern Chile: for a slab age of 50 Ma, the expected interplane distance is ~7 km and not 20–25 km [*Comte et al.*, 1999; *Dorbath et al.*, 2008].

[31] *Dorbath et al.* [2008] proposed that the slab's unusually low thermal structure relative to its age accounts for the northern Chilean DSZ interplane distances. Heat flow studies offshore central Chile show much lower values than predicted (24–31 mW/m^2) [*Grevemeyer et al.*, 2003, 2005] compared to the expected ~90 mW/m^2 for a lithosphere age of ~32 Ma; (*Stein*, [2003]). Since the northern and central Chilean DSZs are far away from another but located within the same slab, all showing unexpectedly large widths, we suggest that, in the case of the Nazca slab, its age is not the direct cause of its DSZs' interplane distances, but rather other factors, such as thermal state, dehydration reactions, and consequent fluid migration, may play an important role.

[32] Considering the impact of plate convergence on the slab, as emphasized by *Fujita and Kanamori* [1981], the central Chile DSZ belongs to what *Kao and Rau* [1999] termed the "type III" model for the Philippine Sea plate DSZ, characterized by compression in the shallow part and extension in the deeper part. In our case, the depth limit of 60–70 km corresponds to the maximum depth of the continental crustal root jamming into the subducting plate. The estimated stress tensor for these depths shows that the slab is undergoing horizontal compression in the upper 60–70 km depth and affecting at least 20–25 km of the slab from its upper surface. The same stress tensor solutions fit the back-arc crust (Figure 7), ~800 km eastward from the trench, emphasizing the large-scale and dominant role of plate convergence in the resulting compressional regime. On the other hand, inferred *P* and *T* axes for the DSZ below 60–70 km depth until the slab fold hinge, where the DSZ seems to disappear, indicate that the slab is dominated by horizontal and slabdip tension. The flat slab segment is in horizontal/slabdip compression with sideways extension influenced by the slab geometry [*Anderson et al.*, 2007]. The Nazca slab's extensional regime between 60 and 70 km and the depth of horizontal subduction can be explained by the fast westward motion of the overriding plate that results in trench retreat [*Lallemand et al.*, 2008] and by its downward loading on the subducting plate, inducing slab stretching which is likely accommodated by reactivation of preexisting faults, as suggested by the dominance in normal focal mechanisms and focal plane striking parallel to the trench axis at these depths. In turn, the slab's compressive regime above 60–70 km depth can be explained by the rapid horizontal plate convergence, strong plate coupling, rapid subduction rate, buoyant lithosphere, and subducting JFR topography.

[33] Dehydration reactions are commonly proposed as a triggering mechanism to explain the presence and characteristics of DSZs [e.g., *Yamasaki and Seno*, 2003; *Hacker et al.*, 2003; *Hacker*, 2008; *van Keken et al.*, 2011]. The central Chilean DSZ shows several characteristics compatible with dehydration reaction patterns: (i) unexpectedly large interplane distance with respect to slab age, (ii) merging of

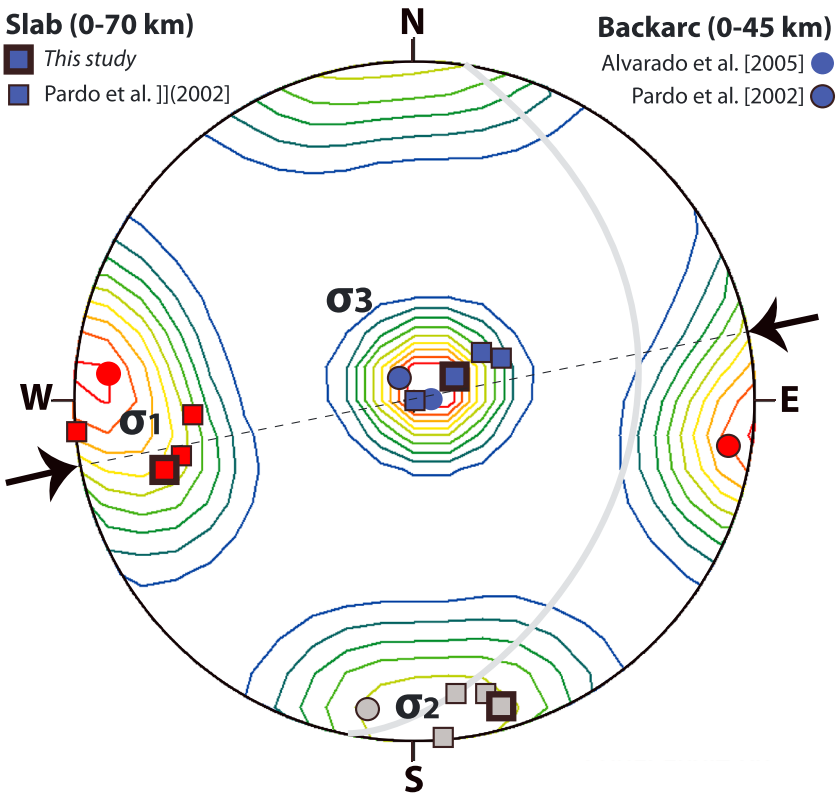

Figure 7. Stress tensor orientations (σ_1: red, σ_2: gray, σ_3: blue) calculated by different studies, projected on a lower hemisphere, showing the similarity in solutions between the slab and the back-arc continental crust. Thick squares represent the stress tensor calculated in this study (shown in Figure 6) for the depth range of 50 to 60–70 km depth. Thin squares represent the stress tensor solutions calculated by *Pardo et al.* [2002] for earthquakes located between 0 and 70 km depths at different latitudes along the flat slab. Circles represent the solutions calculated by *Pardo et al.* [2002] and *Alvarado et al.* [2005] for the continental crust between 0 and 45 km depth. The slab orientation at these latitudes and depths is shown by the thick gray great circle. The black dotted line and arrows denote the azimuth of the plate convergence.

both seismic planes with depth, and (iii) deep-seated seismicity beneath the trench axis at ~40 km depth (Figure 3), as predicted by dehydration paths. If dehydration embrittlement, fluid migration or local weakening [*Dorbath et al.*, 2008; *Faccenda et al.*, 2010], associated to the presence of fluids, are the effective generators of seismicity for the central Chilean DSZ, the Nazca lithosphere must be hydrated down to at least 20–25 km, where we observe the LP. Since dehydration paths for mantle phases do not match the UP seismicity band, it is widely acknowledged that UPs represent the breakdown of oceanic crust (meta-basalts and meta-gabbros; e.g. amphibolites and blueschists) to anhydrous eclogite facies [*Kirby et al.*, 1996; *Peacock et al.*, 2001; *Hacker et al.*, 2003;*van Keken et al.*, 2011]. The continuous and denser seismicity along the LP, compared to the UP, suggests that the role of fluids is more prominent than along the UP, and that dehydration reactions and/or fluid migration are continuously ongoing in time and space.

[34] Evidence of plate hydration in the region is revealed by the low heat flux values offshore central Chile, which reflect active hydrothermal convection along the outer rise [*Grevemeyer et al.*, 2003; 2005]. The region's bathymetry indicates that the outer rise is intensely fractured, as shown by the presence of the following: (i) reactivated seafloor fabric, (ii) trench-parallel faults, and (iii) JFR-parallel faults [*Ranero et al.*, 2005]. Widespread reduced upper mantle velocities beneath and around the JFR axis further indicate that the Nazca Plate is already hydrated before its passage over the outer rise [*Kopp et al.*, 2004]. We have indicated earlier in the discussion that the JFR may be an influencing factor for the DSZ in this region, and, because of the similarities with dehydration reaction paths, we suggest that there is a possible relationship with the JFR's degree and depth of hydration.

[35] Our focal mechanisms for the DSZ below 60–70 km depth indicate a strong tendency for trench-parallel strike orientations (~NS) consistent with the region's outer rise bend faults [*Ranero et al.*, 2005]. Furthermore, their dominant dip is 40°W, amounting to 70°W when accounting for slab dip, which is representative of typical normal faults at Earth's surface. This observation provides evidence that outer rise faults are preserved in the subducting slab and become reactivated around 60–70 km depth in this region [see *Marot et al.*, 2012]. In Middle America, *Warren et al.* [2008] reported the reactivation of outer rise faults at depth ranges of 35–85 km. Dehydration embrittlement, fluid migration, and local weakening [*Dorbath et al.*, 2008; *Faccenda et al.*, 2009, 2012] could be the triggering mechanism for fault plane reactivation at intermediate depths [*Jung et al.*, 2004].

[36] How fluids manage to penetrate the lithosphere to depths of 20–40 km may be accounted for by a model by *Faccenda et al*. [2009] invoking a mechanism of "seismic pumping" which takes place during an event along bend faults and which enhances water migration to deeper levels, down to ~50–70 km depth. The association of plate unbending with dehydration reactions is a hypothesis that was also put forward by *Dorbath et al*. [2008] to explain the northern Chilean DSZ between 18.5°S and 19.5°S and by *Faccenda and Mancktelow* [2010] for global models. These authors propose that fluids trapped in the oceanic mantle are released from the tensile lower part of the slab due to slab unbending, then ascend due to buoyancy, and accumulate at the base of the compressional upper part of the slab. This would create a fluid-rich layer, where pore fluid pressure exceeds a critical threshold and produces seismic failure, accounting for the LPs of DSZs. However, we do not observe the effects of slab unbending along the central Chile DSZ, where the LP is under tension for most of the DSZ's depth extent, probably because the influence of plate interaction is stronger.

[37] The three most commonly evoked dehydrating mantle minerals when discussing global LP occurrences are antigorite, chlorite, and 10 Å-phase. *Fumagalli and Poli* [2005] proposed that antigorite breakdown is responsible for the LPs in water-saturated colder slabs and chlorite-10 Å-phase breakdown in undersaturated hotter slabs. *Fumagalli et al*. [2001] demonstrated that the dehydration of 10 Å-phase, from the breakdown of chlorite and/or talc as P-T conditions increase, results in continuous volatile release rather by discrete fluid pulses, and this process could possibly be responsible for the LP's higher and uninterrupted seismicity. Also, the merging depth between UP and LP depends on the slab's thermal structure and water content. *Yamasaki and Seno* [2003] and *Brudzinski et al*. [2007] matched most DSZs with the breakdown of antigorite and merely a few with chlorite dehydration. The latter cases are associated with anomalously large interplane distances. Furthermore, *Babeyko and Sobolev* [2008] observed that dehydration reactions are mainly temperature driven rather than pressure dependent. This is further evidence that the distance of separation is primarily controlled by the slab's thermal structure rather than absolute age. Hence, the large interplane separation of the central Chilean DSZ could be explained by the slab's thermal structure and consequent preference for the breakdown of chlorite minerals. The depth of merging (~120 km) would be where complete devolatization of the slab occurs [*Fumagalli et al*., 2001].

[38] Because dehydration paths for mantle phases do not match the UP seismicity band, it is widely acknowledged that UPs represent the breakdown of oceanic crust (meta-basalts and meta-gabbros; e.g., amphibolites and blueschists) to anhydrous eclogite facies [*Kirby et al*., 1996; *Peacock*, 2001; *Hacker et al*., 2003; *van Keken et al*., 2011]. These reactions provoke a 10% bulk volume reduction [*Kirby et al*., 1996], which could explain the UP's extensional nature below 60–70 km with crustal stretching and normal faulting.

5. Conclusions

[39] We have reported the geometry and characteristics of the Central Chilean DSZ. Its LP extends continuously 300 km along strike from 29.5°S to 32.5°S, initiates at 50 km depth, has an interplane maximum distance of 20–25 km, and merges with the UP at 100–120 km depth, coincident with the flat slab's fold hinge. Its detection in this region is due to the installation of local seismic networks, and its occurrence is probably related to the subducting JFR and its degree of hydration. However, the relation between the JFR and the DSZ is not entirely clear. The latter southward geographical span appears to end at the abrupt southern transition zone, which we suggest is due to the slab's change in geometry. Its unusually large interplane distance, as for the other DSZs in the Nazca slab, is probably related to the slab's relatively cold thermal structure, compared to its absolute age.

[40] Focal mechanisms show that the slab changes regime at 60–70 km of depth, with predominant compression and tension above and below, respectively, affecting at least the top 20–25 km of the slab from its upper surface. The estimated stress tensors show that both seismic planes of the DSZ are subjected to compression above 60–70 km of depth, due to high plate convergence, and are dominated by horizontal extension parallel to the convergence direction below this depth, due to heavy continental loading of the overriding lithosphere. This depth limit corresponds to the depth of the overriding continental crustal root. These observations allowed us to discredit plate sagging or unbending as the causal mechanisms for this DSZ, since these result in stress partitioning between both seismic planes. Instead, we consider the Central Chilean DSZ another rare example of "type III" DSZ proposed by *Kao and Rau* [1999] for the Philippine Sea plate, where strong convergence with a thick continental crust dominates the slab's stress regime at intermediate depth.

[41] The DSZ shape, like all other global occurrences, shows strong resemblances with dehydration reaction paths. Evidence that the central Chilean Nazca slab is hydrated prior to subduction comes not only from offshore seismic surveys indicating reduced mantle velocities and high electrical conductivity but also from our observation that focal mechanism strike orientations below 60–70 km of depth strongly correlate with regional outer rise fault strikes. This suggests that reactivation of inherited outer rise faults dominates below ~60–70 km depth until at least 120 km depth, where merging of the two seismic planes occurs.

[42] In agreement with other hypotheses, we propose that dehydration embrittlement, fluid migration, or local weakening provide the mechanism necessary to weaken rocks/faults, while the ambient stress field controls the occurrence and orientation of rupture. In this context, global DSZ occurrences and interplane distances can be explained by the slab's thermal structure and volatile content.

[43] **Acknowledgments.** We are grateful to Bertrand Delouis for his collaboration and help in the use of his code of stress tensor inversion. We thank Perrine Deshayes for notifying the central Chilean DSZ in her PhD thesis. We are equally thankful to all people who have participated in active discussions on the subject with us and have brought us new insights into the topic. Local data were obtained thanks to projects FONDECYT 1020972-1050758 and IRD-GéoAzur, and the unconditional logistic support of INPRES in the field trips in Western Argentina. Marianne Marot and Guust Nolet are supported by the GlobalSeis project (ERC 226837). Giorgio Ranalli's participation in this project is supported by a grant by NSERC (Natural Sciences and Engineering Research Council of Canada). We thank two anonymous reviewers whose thoughtful comments have helped us to prepare the final version of this paper.

References

Alvarado, P., S. Beck, G. Zandt, M. Araujo, and E. Triep (2005), Crustal deformation in the south-central Andes backarc terranes as viewed from regional broad-band seismic waveform modeling, *Geophys. J. Int.*, *163*(2), 580–598, doi:10.1111/j.1365-246X.2005.02759.x.

Anderson, M., P. Alvarado, G. Zandt, and S. Beck (2007), Geometry and brittle deformation of the subducting Nazca Plate, Central Chile and Argentina, *Geophys. J. Int.*, *171*(1), 419–434, doi:10.1111/j.1365-246X.2007.03483.x.

Araujo, M., and G. Suárez (1994), Geometry and state of stress of the subducted Nazca Plate beneath central Chile and Argentina: Evidence from teleseismic data, *Geophys. J. Int.*, *116*(2), 283–303, doi:10.1111/j.1365-246X.1994.tb01799.x.

Babeyko, A. Y., and S. V. Sobolev (2008), High-resolution numerical modeling of stress distribution in visco-elasto-plastic subducting slabs, *Lithos*, *103*(1), 205–216, doi:10.1016/j.lithos.2007.09.015.

Barazangi, M., and B. L. Isacks (1976), Spatial distribution of earthquakes and subduction of the Nazca Plate beneath South America, *Geology*, *4*(11), 686–692, doi:10.1130/0091-7613(1976).

Brudzinski, M. R., C. H. Thurber, R. Hacker, and E. R. Engdahl (2007), Global prevalence of double Benioff zones, *Science*, *316*(5830), 1472–1474, doi:10.1126/science.1139204.

Cahill, T., and B. L. Isacks (1992), Seismicity and shape of the subducted Nazca Plate, *J. Geophys. Res.*, *97*(B12), 17,503–17,529.

Campos, J., D. Hatzfeld, R. Madiagara, G. López, E. Kausel, A. Zollo, G. Iannacone, R. Fromm, S. Barrientos, and H. Lyon-Caen (2002), A seismological study of the 1835 seismic gap in south-central Chile, *Phys. Earth Planet. Inter.*, *132*(1), 177–195, doi:10.1016/S0031-9201(02)00051-1.

Clouard, V., J. Campos, A. Lemoine, A. Perez, and E. Kausel (2007), Outer rise stress changes related to the subduction of the Juan Fernandez Ridge, central Chile, *J. Geophys. Res.*, *112*, B05305, doi:10.1029/2005JB0033999.

Comte, D., and G. Suárez (1994), An inverted double seismic zone in Chile: Evidence of phase transformation in the subducted slab, *Science*, *263*(5144), 212–215, doi:10.1126/science.263.5144.212.

Comte, D., L. Dorbath, M. Pardo, T. Monfret, H. Haessler, L. Rivera, M. Frogneux, B. Glass, and C. Meneses (1999), A double-layered seismic zone in Arica, northern Chile, *Geophys. Res. Lett.*, *26*(13), 1965–1968, doi:10.1029/1999GL900447.

Delouis, B., J. Déverchère, V. Melnikova, N. Radziminovitch, L. Loncke, C. Larroque, J. F. Ritz, and V. San'kov (2002), A reappraisal of the 1950 (*Mw* 6.9) Mondy earthquake, Siberia, and its relationship to the strain pattern at the south-western end of the Baikal rift zone, *Terra Nova*, *14*(6), 491–500.

Dorbath, C., M. Gerbault, G. Carlier, and M. Guiraud (2008), Double seismic zone of the Nazca Plate in northern Chile: High-resolution velocity structure, petrological implications, and thermomechanical modeling, *Geochem. Geophys. Geosyst.*, *9*, Q07006, doi:10.1029/2008GC002020.

Engdahl, E. R., and C. H. Scholz (1977), A double Benioff zone beneath the central Aleutians: An unbending of the lithosphere, *Geophys. Res. Lett.*, *4*, 473–476, doi:10.1029/GL004i010p00473.

Engdahl, E. R., R. van der Hilst, and R. Buland (1998), Global teleseismic earthquake relocation with improved travel times and procedures for depth determination, *Bull. Seismol. Soc. Am.*, *88*(3), 722–743.

Faccenda, M., and N. S. Mancktelow (2010), Fluid flow during unbending: Implications for slab hydration, intermediate-depth earthquakes and deep fluid subduction, *Tectonophysics*, *494*(1), 149–154, doi:10.1016/j.tecto.2010.08.002.

Faccenda, M., T. V. Gerya, and L. Burlini (2009), Deep slab hydration induced by bending-related variations in tectonic pressure, *Nat. Geosci.*, *2*(11), 790–793, doi:10.1038/NGEO656.

Faccenda, M., T. V. Gerya, N. S. Mancktelow, and L. Moresi (2012), Fluid flow during slab unbending and dehydration: Implications for intermediate-depth seismicity, slab weakening and deep water recycling, *Geochem. Geophys. Geosyst.*, *13*, Q01010, doi:10.1029/2011GC003860.

Fromm, R., G. Zandt, and S. L. Beck (2004), Crustal thickness beneath the Andes and Sierras Pampeanas at 30°S inferred from Pn apparent phase velocities, *Geophys. Res. Lett.*, *31*, L06625, doi:10.1029/2003GL019231.

Fry, A., N. Kusznir, M. Dabrowski, A. Rietbrock, and I. Podladtchikov (2009), Modelling stress accumulation and dissipation and the causes of intermediate-depth seismicity in subduction zones, *Geophys. Res. Abstr.*, *11*, EGU2009–8382.

Fujita, K., and H. Kanamori (1981), Double seismic zones and stresses of intermediate depth earthquakes, *Geophys. J. Int.*, *66*(1), 131–156, doi:10.1111/j.1365-246X.1981.tb05950.x.

Fumagalli, P., and S. Poli (2005), Experimentally determined phase relations in hydrous peridotites to 6.5 GPa and their consequences on the dynamics of subduction zones, *J. Petrol.*, *46*(3), 555–578, doi:10.1093/petrology/egh088.

Fumagalli, P., L. Stixrude, S. Poli, and D. Snyder (2001), The 10 Å-phase: A high-pressure expandable sheet silicate stable during subduction of hydrated lithosphere, *Earth Planet. Sci. Lett.*, *186*(2), 125–141, doi:10.1016/S0012-821X(01)00238-2.

Gilbert, H., S. Beck, and G. Zandt (2006), Lithospheric and upper mantle structure of central Chile and Argentina, *Geophys. J. Int.*, *165*(1), 383–398, doi:10.1111/j.1365-246X.2006.02867.x.

Grevemeyer, I., J. L. Diaz-Naveas, C. R. Ranero, and H. W. Villinger (2003), Heat flow over the descending Nazca Plate in central Chile, 32°S to 41°S: Observations from ODP Leg 202 and the occurrence of natural gas hydrates, *Earth Planet. Sci. Lett.*, *213*(3), 285–298, doi:10.1016/S0012-821X(03)00303-0.

Grevemeyer, I., N. Kaul, J. L. Diaz-Naveas, H. W. Villinger, C. R. Ranero, and C. Reichert (2005), Heat flow and bending-related faulting at subduction trenches: Case studies offshore of Nicaragua and Central Chile, *Earth Planet. Sci. Lett.*, *236*(1), 238–248, doi:10.1016/j.epsl.2005.04.048.

Haberland, C., A. Rietbrock, D. Lange, K. Bataille, and T. Dahm (2009), Structure of the seismogenic zone of the southcentral Chilean margin revealed by local earthquake traveltime tomography, *J. Geophys. Res.*, *114*, B01317, doi:10.1029/2008JB005802.

Hacker, B. R. (2008), H_2O subduction beyond arcs, *Geochem. Geophys. Geosyst.*, *9*, Q03001, doi:10.1029/2007GC001707.

Hacker, B. R., S. M. Peacock, G. A. Abers, and S. D. Holloway (2003), Subduction factory: 2. Are intermediate-depth earthquakes in subducting slabs linked to metamorphic dehydration reactions?, *J. Geophys. Res.*, *108*(B1), 2030, doi:10.1029/2001JB001129.

Hasegawa, A., N. Umino, and A. Takagi (1978), Double planed deep seismic zone and upper mantle structure in the northeastern Japan arc, *Geophys. J. R. Astron. Soc.*, *54*, 281–296, doi:10.1111/j.1365-246X.1978.tb04260.x.

Heit, B., X. Yuan, M. Bianchi, F. Sodoudi, and R. Kind (2008), Crustal thickness estimation beneath the southern central Andes at 30°S and 36° S from S wave receiver function analysis, *Geophys. J. Int.*, *174*(1), 249–254, doi:10.1111/j.1365-246X.2008.03780.x.

Heuret, A., and S. Lallemand (2005), Plate motions, slab dynamics and back-arc deformation, *Phys. Earth Planet. Inter.*, *149*(1), 31–51.

Heuret, A., F. Funiciello, C. Faccenna, and S. Lallemand (2007), Plate kinematics, slab shape and back-arc stress: A comparison between laboratory models and current subduction zones, *Earth Planet. Sci. Lett.*, *256*(3), 473–483, doi:10.1016/j.epsl.2007.02.004.

Isacks, B. L., and M. Barazangi (1977), Geometry of Benioff zones: Lateral segmentation and downwards bending of the subducted lithosphere, in *Island Arcs, Deep Sea Trenches and Back-Arc Basins, Maurice Ewing Ser.*, vol. *1*, edited by M. Talwani and W. C. Pitman III, pp. 99–114, AGU, Washington, D. C., doi:10.1029/ME001p0099.

Jordan, T. E., B. L. Isacks, R. W. Allmendinger, J. A. Brewer, V. A. Ramos, and C. J. Ando (1983), Andean tectonics related to geometry of the subducted Nazca plate, *Geol. Soc. Am. Bull.*, *94*(3), 341–361, doi:10.1130/0016-7606(1983)94<341:ATRTGO.

Jung, H., H. W. Green II, and L. F. Dobrzinetskaya (2004), Intermediate-depth earthquake faulting by dehydration embrittlement with negative volume change, *Nature*, *428*, 545–549, doi:10.1038/nature02412.

Kao, H., and W. P. Chen (1994), The double seismic zone in Kuril-Kamchatka: The tale of two overlapping single zones, *J. Geophys. Res.*, *99*, 6913–6930.

Kao, H., and R. J. Rau (1999), Detailed structures of the subducted Philippine Sea plate beneath northeast Taiwan: A new type of double seismic zone, *J. Geophys. Res.*, *104*, 1015–1033, doi:10.1029/1998JB900010.

Kawakatsu, H., and T. Seno (1983), Triple seismic zone and the regional variation of seismicity along the Northern Honshu arc, *J. Geophys. Res.*, *88*, 4215–4230.

Kay, S., V. Maksaev, R. Moscoso, C. Mpodozis, and C. Nasi (1987), Probing the evolving Andean lithosphere: Mid-late Tertiary magmatism in Chile (29°–30°30′S) over the modern zone of subhorizontal subduction, *J. Geophys. Res.*, *92*, 6173–6189.

Kendrick, E., M. Bevis, R. Smalley Jr., B. Brooks, R. B. Vargas, E. Lauria, and L. P. Souto Fortes (2003), The Nazca-South America Euler vector and its rate of change, *J. South Am. Earth Sci.*, *16*, 125–131, doi:10.1016/S0895-9811(03)00028-2.

Kirby, S., R. Enghdal, and R. Benlinger (1996), Intermediate-depth intraslab earthquakes and arc-volcanism as physical expression of crustal and uppermost mantle metamorphism in subducting slabs, in *Subduction: Top to Bottom*, *Geophys. Monogr. Ser.*, vol. *96*, edited by G. Bedout et al., pp. 195–214, AGU, Washington, D. C., doi:10.1029/GM096p0195.

Kissling, E., W. L. Ellsworth, D. Eberhart-Phillips, and U. Kradolfer (1994), Initial reference models in local earthquake tomography, *J. Geophys. Res.*, *99*(B10), 19,635–19,646.

Kopp, H., R. Flueh, C. Papenberg, and D. Klaeschen (2004), Seismic investigations of the O'Higgins Seamount Group and Juan Fernandez Ridge: Aseismic ridge emplacement and lithosphere hydration, *Tectonics*, *23*, TC2009, doi:10.1029/2003TC001590.

Lallemand, S., A. Heuret, C. Faccenna, and F. Funiciello (2008), Subduction dynamics as revealed by trench migration, *Tectonics*, *27*, TC3014, doi:10.1029/2007YC002212.

Lay, T., and T. C. Wallace (1995), *Modern Global Seismology*, vol. *58*, 517 pp., Academic, New York.

Lowrie, A., and R. Hey (1981), Geological and geophysical variations along the western margin of Chile near lat 33° to 36°S and their relation to Nazca Plate subduction, in *Nazca Plate: Crustal Formation and Andean Convergence, Mem.*, *Geol. Soc. Am., Memoir*, *154*, 741–754.

Marot, M., T. Monfret, M. Pardo, G. Ranalli, and G. Nolet (2012), An intermediate-depth tensional earthquake (M_w 5.7) and its aftershocks within the Nazca Plate, central Chile: A reactivated outer rise fault?, *Earth Planet. Sci. Lett.*, *327*, 9–16, doi:10.1016/j.epsl.2012.02.003.

Martinod, J., F. Funiciello, C. Faccenna, S. Labanieh, and V. Regard (2005), Dynamical effects of subducting ridges: Insights from 3-D laboratory models, *Geophys. J. Int.*, *163*(3), 1137–1150, doi:10.1111/j.1365-246X.2005.02797.x.

Martinod, J., L. Husson, P. Roperch, B. Guillaume, and N. Espurt (2010), Horizontal subduction zones, convergence velocity and the building of the Andes, *Earth Planet. Sci. Lett.*, *299*(3), 299–309, doi:10.1016/j.epsl.2010.09.010.

McGuire, J. J., and D. A. Wiens (1995), A double seismic zone in New Britain and the morphology of the Solomon plate at intermediate-depths, *Geophys. Res. Lett.*, *22*, 1965–1968, doi:10.1029/95GL01806.

Montelli, R., G. Nolet, F. A. Dahlen, G. Maters, E. R. Engdahl, and S. H. Hung (2004), Finite-frequency tomography reveals a variety of plumes in the mantle, *Science*, *303*, 338–343, doi:10.1126/science.1092485.

Müller, R. D., W. R. Roest, J.-Y. Royer, L. M. Grahagan, and J. G. Sclater (1997), Digital isochrones of the world's sea floor, *J. Geophys. Res.*, *102*, 3211–3214.

Pardo, M., D. Comte, and T. Monfret (2002), Seismotectonic and stress distribution in the central Chile subduction zone, *J. South Am. Earth Sci.*, *15*(1), 11–22, doi:10.1016/S0895-9811(02)00003-2.

Pardo, M., T. Monfret, E. Vera, G. Yáñez, and A. Eisenberg (2004), Flat slab to steep subduction transition zone in central Chile-western Argentina: Body waves tomography and state of stress, *Eos Trans. AGU*, *85*(47), Fall Meet. Suppl., Abstract S51B-0164.

Peacock, S. M. (2001), Are the lower planes of double seismic zones caused by serpentine dehydration in subducting oceanic mantle?, *Geology*, *29*(4), 299–302.

Pesicek, J. D., E. R. Engdahl, C. H. Thurber, H. R. DeShon, and D. Lange (2012), Mantle subducting slab structure in the region of the 2010 M 8.8 Maule earthquake (30°–40°S), Chile, *Geophys. J. Int.*, *191*(1), 317–324.

Pilger, R. H., Jr. (1981), Plate reconstructions, aseismic ridges, and low angle subduction beneath the Andes, *Geol. Soc. Am. Bull.*, *92*, 448–456, doi:10.1130/0016-7606.

Prevot, R., J.-L. Chatelain, S. W. Roecker, and J.-R. Grasso (1994), A shallow double seismic zone beneath the central New Hebrides (Vanuatu): Evidence for fragmentation and accretion of the descending plate, *Geophys. Res. Lett.*, *21*, 2159–2162.

Ramos, V. A., E. O. Cristallini, and D. J. Pérez (2002), The Pampean flat-slab of the Central Andes, *J. South Am. Earth Sci.*, *15*(1), 59–78, doi:10.1016/S0895-9811(02)00006-8.

Ranero, C. R., A. Villasenor, J. P. Morgan, and W. Weinrebe (2005), Relationship between bend-faulting at trenches and intermediate-depth seismicity, *Geochem. Geophys. Geosyst.*, *6*, Q12002, doi:10.1029/2005GC000997.

Ratchkovsky, N. A., J. Pujol, and N. N. Biswas (1997), Stress pattern in the double seismic zone beneath Cook Inlet, south-central Alaska, *Tectonophysics*, *281*(3), 163–171, doi:10.1016/S0040-1951(97)00042-5.

Rietbrock, A., and F. Waldhauser (2004), A narrowly double-seismic zone in the subducted Nazca Plate, *Geophys. Res. Lett.*, *31*, L10608, doi:10.1029/2004GL019610.

Rivera, L., and A. Cisternas (1990), Stress tensor and fault plane solutions for a population of earthquakes, *Bull. Seismol. Soc. Am.*, *80*(3), 600–614.

Robinson, R. (1986), Seismicity, structure and tectonics of the Wellington region, New Zealand, *Geophys. J. R. Astron. Soc.*, *87*(2), 379–409, doi:10.1111/j.1365-246X.1986.tb06629.x.

Salazar, P. (2005), Análisis del campo de esfuerzos en la zona de subducción bajo Chile Central (30°–34°S) [in Spanish], doctoral dissertation, M. Sc. thesis, 196 pp., Univ. of Chile, Santiago.

Seno, T., and B. Pongsawat (1981), A triple-planed structure of seismicity and earthquake mechanisms at the subduction zone of Miyagi Prefecture, northern Honshu, Japan, *Earth Planet. Sci. Lett.*, *55*(1), 25–36, doi:10.1016/0012-821X(81)90083-2.

Seno, T., D. Zhao, Y. Kobayashi, and M. Nakamura (2001), Dehydration of serpentinized slab mantle: Seismic evidence from southwest Japan, *Earth Planets Space*, *53*(9), 861–872.

Shiobara, H., H. Sugioka, K. Mochizuki, S. Oki, T. Kanazawa, Y. Fukao, and K. Suyehiro (2010), Double seismic zone in the North Mariana region revealed by long-term ocean bottom array observation, *Geophys. J. Int.*, *183*(3), 1455–1469, doi:10.1111/j.1365-246X.2010.04799.x.

Smalley, R. F., Jr., and B. L. Isacks (1987), A high-resolution local network study of the Nazca Plate Wadati-Benioff zone under Western Argentina, *J. Geophys. Res.*, *92*, 13,903–13,912.

Snoke, J. A., J. W. Munsey, A. G. Teague, and G. A. Bollinger (1984), A program for focal mechanism determination by combined use of polarity and SV-P amplitude ratio data, *Earthquake Notes*, *55*(3), 15–20.

Stein, C. A. (2003), Heat flow and flexure at subduction zones, *Geophys. Res. Lett.*, *30*(23), 2197, doi:10.1029/2003GL018478.

Syracuse, E. M., P. E. van Keken, and G. A. Abers (2010), The global range of subduction zone thermal models, *Phys. Earth Planet. Inter.*, *183*(1), 73–90, doi:10.1016/j.pepi.2010.02.004.

Tassara, A., and A. Echaurren (2012), Anatomy of the Andean subduction zone: Three-dimensional density model upgraded and compared against global-scale models, *Geophys. J. Int.*, *189*(1), 161–168, doi:10.1111/j.1365-246X.2012.05397.x.

Tassara, A., H. J. Götze, S. Schmidt, and R. Hackney (2006), Three-dimensional density model of the Nazca plate and the Andean continental margin, *J. Geophys. Res.*, *111*, doi:10.1029/2005JB003976.

van Keken, P. E., B. R. Hacker, E. M. Syracuse, and G. A. Abers (2011), Subduction factory: 4. Depth-dependent flux of H_2O from subducting slabs worldwide. *J. Geophys. Res.*, *116*, B01401, doi:10.1029/2010JB007922.

Wada, I., and K. Wang (2009), Common depth of slab-mantle decoupling: Reconciling diversity and uniformity of subduction zones, *Geochem. Geophys. Geosyst.*, *10*, Q10009, doi:10.1029/2009GC002570.

Waldhauser, F., and W. L. Ellsworth (2000), A double-difference earthquake location algorithm: Method and application to the northern Hayward fault, California, *Bull. Seismol. Soc. Am.*, *90*(6), 1353–1368.

Wang, K., and G. C. Rogers (1994), An explanation for the double seismic layers north of the Mendocino triple junction, *Geophys. Res. Lett.*, *21*(2), 121–124.

Warren, L. M., M. A. Langstaff, and P. G. Silver (2008), Fault plane orientations of intermediate-depth earthquakes in the Middle America trench, *J. Geophys. Res.*, *113*, B01304, doi:10.1029/2007JB005028.

Yamasaki, T., and T. Seno (2003), Double seismic zone and dehydration embrittlement of the subducting slab, *J. Geophys. Res.*, *108*(B4), 2212, doi:10.1029/2002JB001918.

Yáñez, G., J. Cembrano, M. Pardo, C. Ranero, and D. Selles (2002), The Challenger-Juan Fernández-Maipo major tectonic transition of the Nazca-Andean subduction system at 33°–34°S: Geodynamic evidence and implications, *J. South Am. Earth Sci.*, *15*(1), 23–28, doi:10.1016/S0895-9811(02)00004-4.

Zhao, D. (2007), Seismic images under 60 hotspots: Search for mantle plumes, *Gondwana Res.*, *12*(4), 335–355, doi:10.1016/j.gr.2007.03.001.